Recent results of the CMS experiment

Dr. Bora Akgün[1]

Rice University, Physics and Astronomy Department
6100 Main Street, Houston, Texas, USA

Recent results of the CMS experiment has been reviewed. Selected results cover a variety of topics including rare $B_s^0 \rightarrow \mu^+\mu^-$ decay from combined analysis of CMS and LHCb, prompt J/ψ and $\psi(2S)$ double-differential cross sections, differential cross section for top quark pair production and a search for physics beyond the standard model in events with two leptons, jets, and missing transverse momentum.

1 CMS detector

The central feature of the CMS apparatus is a superconducting solenoid of 13 m length 6 m internal diameter having a 3.8 T field. Within the superconducting solenoid volume are a silicon pixel and strip tracker, a lead tungstate crystal electromagnetic calorimeter, and a brass and scintillator hadron calorimeter. Muons are measured in gas-ionization detectors embedded in the steel flux-return yoke outside the solenoid, with detection planes are made using three technologies: drift tubes, cathode strip chambers, and resistive-plate chambers. Muons are measured in the pseudorapidity range $|\eta| < 2.4$.

The silicon tracker measures charged particles within the pseudorapidity range $|\eta| < 2.5$. It consists of 1440 silicon pixel and 15148 silicon strip detector modules and provides a typical transverse impact parameter resolution of 25–90 μm.

The first level of the CMS trigger system, composed of custom hardware processors, uses information from the calorimeters and muon detectors to select the most interesting events in a fixed time interval of less than 4μs. The high-level trigger processor farm further decreases the event rate from around 100 kHz to around 400 Hz, before data storage. A more detailed description of the CMS detector, together with a definition of the coordinate system used and the relevant kinematic variables, can be found in Ref. [1].

2 Observation of the rare $B_s^0 \rightarrow \mu^+\mu^-$ decay from the combined analysis of CMS and LHCb data

The standard model of particle physics describes the fundamental particles and their interactions via the strong, electromagnetic, and weak forces. It provides precise predictions for measurable quantities that can be tested experimentally. The probabilities, or branching fractions, of the B_s^0 and the B^0 meson decaying into two oppositely charged muons (μ^+ and μ^-) are especially interesting because of their sensitivity to theories that extend the standard model. The standard model predicts that the $B_s^0 \rightarrow \mu^+\mu^-$ and $B^0 \rightarrow \mu^+\mu^-$ decays are very rare, with about four of the former occurring for every billion B_s^0 mesons produced and one of the latter occurring for every 10 billion B^0 mesons [2]. A difference in the observed branching fractions

---

[1]bora.akgun@cern.ch

with respect to the predictions of the standard model would provide a direction in which the standard model should be extended. Before the Large Hadron Collider (LHC) at CERN [3] started operating, no evidence for either decay mode had been found. Upper limits on the branching fractions were an order of magnitude above the standard model predictions. The CMS (Compact Muon Solenoid) and LHCb (Large Hadron Collider beauty) collaborations have performed a joint analysis of the data from proton-proton collisions that they collected in 2011 at a centre-of-mass energy of 7 TeV and in 2012 at 8 TeV. Here the first observation of the $B_s^0 \to \mu^+\mu^-$ decay is reported, with a statistical significance exceeding six standard deviations, and the best measurement so far of its branching fraction. Furthermore evidence for the $B^0 \to \mu^+\mu^-$ decay with a statistical significance of three standard deviations is obtained. Both measurements are statistically compatible with standard model predictions and allow stringent constraints to be placed on theories beyond the standard model.

The experiments follow similar data analysis strategies. Decays compatible with $B_s^0 \to \mu^+\mu^-$ (candidate decays) are found by combining the reconstructed trajectories (tracks) of oppositely charged particles identified as muons. The separation between genuine $B_s^0 \to \mu^+\mu^-$ decays and random combinations of two muons (combinatorial background), most often from semi-leptonic decays of two different b hadrons, is achieved using the dimuon invariant mass, $m_{\mu^+\mu^-}$, and the established characteristics of B_s^0-meson decays. For example, because of their lifetimes of about 1.5 ps and their production at the LHC with momenta between a few GeV and $\sim 100 GeV$, B_s^0 mesons travel up to a few centimetres before they decay. Therefore, the $B_s^0 \to \mu^+\mu^-$ 'decay vertex', from which the muons originate, is required to be displaced with respect to the 'production vertex', the point where the two protons collide. Furthermore, the negative of the B_s^0 candidate's momentum vector is required to point back to the production vertex.

These criteria, amongst others that have some ability to distinguish known signal events from background events, are combined into boosted decision trees (BDT) [4–6]. A BDT is an ensemble of decision trees each placing different selection requirements on the individual variables to achieve the best discrimination between 'signal-like' and 'background-like' events. Both experiments evaluated many variables for their discriminating power and each chose the best set of about ten to be used in its respective BDT. These include variables related to the quality of the reconstructed tracks of the muons; kinematic variables such as transverse momentum (with respect to the beam axis) of the individual muons and of the B_s^0 candidate; variables related to the decay vertex topology and fit quality, such as candidate decay length; and isolation variables, which measure the activity in terms of other particles in the vicinity of the two muons or their displaced vertex. A BDT must be 'trained' on collections of known background and signal events to generate the selection requirements on the variables and the weights for each tree. In the case of CMS, the background events used in the training are taken from intervals of dimuon mass above and below the signal region in data, while simulated events are used for the signal. The data are divided into disjoint sub-samples and the BDT trained on one sub-sample is applied to a different sub-sample to avoid any bias. LHCb uses simulated events for background and signal in the training of its BDT. After training, the relevant BDT is applied to each event in the data, returning a single value for the event, with high values being more signal-like. To avoid possible biases, both experiments kept the small mass interval that includes both the B_s^0 and B^0 signals blind until all selection criteria were established.

In addition to the combinatorial background, specific b-hadron decays, such as $B^0 \to \pi^-\mu^+\nu$ where the neutrino cannot be detected and the charged pion is misidentified as a muon, or $B^0 \to \pi^0\mu^+\mu^-$, where the neutral pion in the decay is not reconstructed, can mimic the dimuon decay of the B_s^0 mesons. The invariant mass of the reconstructed dimuon candidate for these processes (semi-leptonic background) is usually smaller than the mass of the B_s^0 or B^0 meson because the neutrino or another particle is not detected. There is also a background component from hadronic two-body B_s^0 decays (peaking background) a $B^0 \to K^+\mu^-$, when both hadrons from the decay are misidentified as muons. These misidentified decays can
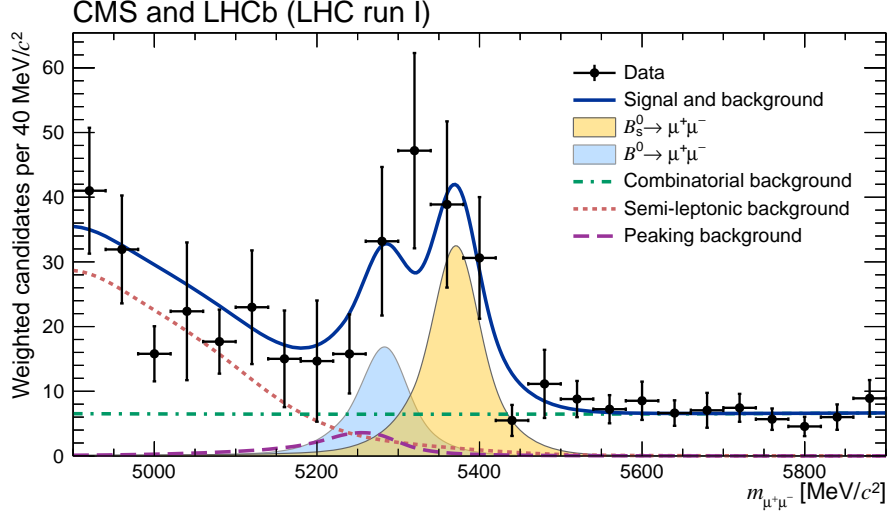
Figure 1: **Weighted distribution of the dimuon invariant mass, $m_{\mu^+\mu^-}$, for all categories.** Superimposed on the data points in black are the combined fit (solid blue line) and its components: the B_s^0 (yellow shaded area) and B^0 (light-blue shaded area) signal components; the combinatorial background (dash-dotted green line); the sum of the semi-leptonic backgrounds (dotted salmon line); and the peaking backgrounds (dashed violet line). The horizontal bar on each histogram point denotes the size of the binning, while the vertical bar denotes the 68% confidence interval. See main text for details on the weighting procedure.

produce peaks in the dimuon invariant-mass spectrum near the expected signal, especially for the $B^0 \rightarrow \mu^+\mu^-$ decay. Particle identification algorithms are used to minimise the probability that pions and kaons are misidentified as muons, and thus suppress these background sources. Excellent mass resolution is mandatory for distinguishing between B^0 and B_s^0 mesons with a mass difference of about 87 MeV and for separating them from backgrounds. The mass resolution for $B_s^0 \rightarrow \mu^+\mu^-$ decays in CMS ranges from 32 to 75 MeV, depending on the direction of the muons relative to the beam axis, while LHCb achieves a uniform mass resolution of about 25 MeV.

The CMS and LHCb data are combined by fitting a common value for each branching fraction to the data from both experiments. The branching fractions are determined from the observed numbers, efficiency-corrected, of B_s^0 mesons that decay into two muons and the total numbers of B_s^0 mesons produced.

In the simultaneous fit to both the CMS and LHCb data, the branching fractions of the two signal channels are common parameters of interest and are free to vary. Other parameters in the fit are considered as nuisance parameters.To represent the result of the fit in a single dimuon invariant-mass spectrum, the mass distributions of all categories, weighted according to values of $S/(S + B)$, where S is the expected number of B_s^0 signals and B is the number of background events under the B_s^0 peak in that category, are added together and shown in Fig. 1.

The combined fit leads to the measurements $\mathcal{B}(B_s^0 \rightarrow \mu^+\mu^-) = 2.8^{+0.7}_{-0.6}$ and $\mathcal{B}(B^0 \rightarrow \mu^+\mu^-) = 3.9^{+1.6}_{-1.4}$, where the uncertainties include both statistical and systematic sources, the latter contributing 35% and 18% of the total uncertainty for the B_s^0 and B^0 signals, respectively.

The fit for the ratios of the branching fractions relative to their SM predictions yields $\mathcal{S}_{SM}^{B_s^0} = 0.76^{+0.20}_{-0.18}$ and $\mathcal{S}_{SM}^{B^0} = 3.7^{+1.6}_{-1.4}$.

The combined analysis of data from CMS and LHCb, taking advantage of their full statistical power, establishes conclusively the existence of the $B_s^0 \to \mu^+\mu^-$ decay and provides an improved measurement of its branching fraction. This concludes a search that started more than three decades ago, and initiates a phase of precision measurements of the properties of this decay. It also produces a three standard deviation evidence for the $B^0 \to \mu^+\mu^-$ decay. The measured branching fractions of both decays are compatible with SM predictions. This is the first time that the CMS and LHCb collaborations have performed a combined analysis of sets of their data in order to obtain a statistically significant observation.

3   Measurement of prompt J/ψ and ψ(2S) double-differential cross sections in pp collisions at $\sqrt{s}$ = 7 TeV

Studies of heavy-quarkonium production are of central importance for an improved understanding of nonperturbative quantum chromodynamics (QCD) [7]. The nonrelativistic QCD (NRQCD) effective-field-theory framework [8], arguably the best formalism at this time, factorizes high-p_T quarkonium production in short-distance and long-distance scales. First a heavy quark-antiquark pair, $Q\overline{Q}$, is produced in a Fock state $^{2S+1}L_J^{[a]}$, with spin S, orbital angular momentum L, and total angular momentum J that are either identical to (color singlet, $a = 1$) or different from (color octet, $a = 8$) those of the corresponding quarkonium state. The $Q\overline{Q}$ cross sections are determined by short-distance coefficients (SDC), kinematic-dependent functions calculable perturbatively as expansions in the strong-coupling constant α_s. Then this "preresonant" $Q\overline{Q}$ pair binds into the physically observable quarkonium through a nonperturbative evolution that may change L and S, with bound-state formation probabilities proportional to long-distance matrix elements (LDME). The LDMEs are conjectured to be constant (i.e., independent of the $Q\overline{Q}$ momentum) and universal (i.e., process independent). The color-octet terms are expected to scale with powers of the heavy-quark velocity in the $Q\overline{Q}$ rest frame. In the nonrelativistic limit, an S-wave vector quarkonium state should be formed from a $Q\overline{Q}$ pair produced as a color singlet ($^3S_1^{[1]}$) or as one of three color octets ($^1S_0^{[8]}$, $^3S_1^{[8]}$, and $^3P_J^{[8]}$).

Three "global fits" to measured quarkonium data [9–11] obtained incompatible octet LDMEs, despite the use of essentially identical theory inputs: next-to-leading-order (NLO) QCD calculations of the singlet and octet SDCs. The disagreement stems from the fact that different sets of measurements were considered. In particular, the results crucially depend on the minimum p_T of the fitted measurements [12], because the octet SDCs have different p_T dependences. Fits including low-p_T cross sections lead to the conclusion that, at high p_T, quarkonium production should be dominated by transversely polarized octet terms. This prediction is in stark contradiction with the unpolarized production seen by the CDF [13, 14] and CMS [15, 16] experiments, an observation known as the "quarkonium polarization puzzle". As shown in Ref. [12], the puzzle is seemingly solved by restricting the NRQCD global fits to high-p_T quarkonia, indicating that the presently available fixed-order calculations provide SDCs unable to reproduce reality at lower p_T values or that NRQCD factorization only holds for p_T values much larger than the quarkonium mass. The polarization measurements add a crucial dimension to the global fits because the various channels have remarkably distinct polarization properties: in the helicity frame, $^3S_1^{[1]}$ is longitudinally polarized, $^1S_0^{[8]}$ is unpolarized, $^3S_1^{[8]}$ is transversely polarized, and $^3P_J^{[8]}$ has a polarization that changes significantly with p_T. Measurements of prompt charmonium cross sections extending well beyond p_T = 50 GeV will trigger improved NRQCD global fits, restricted to a kinematic domain where the factorization formalism is unquestioned, and will provide more accurate and reliable LDMEs.

The analysis is made in four bins of absolute rapidity ($|y| < 0.3$, $0.3 < |y| < 0.6$, $0.6 < |y| < 0.9$, and $0.9 < |y| < 1.2$)
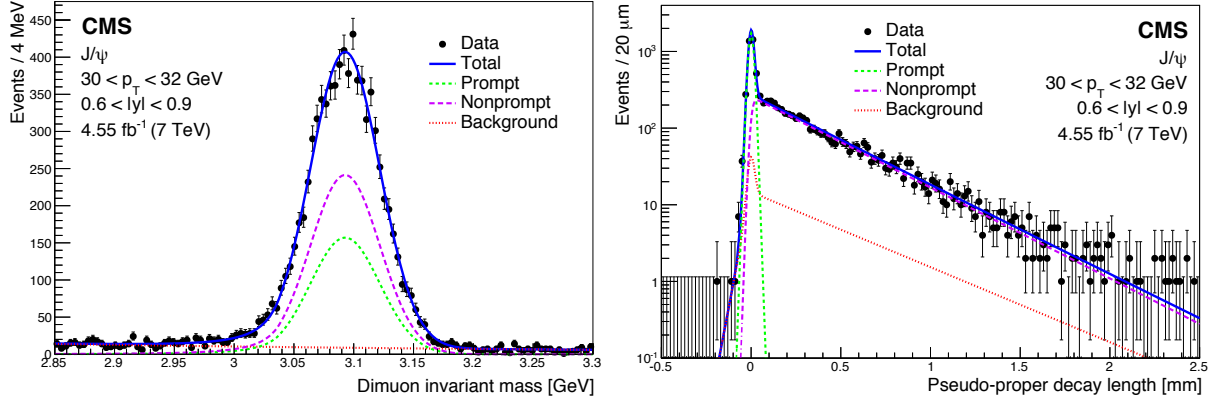
Figure 2: Projections on the dimuon invariant mass (left) and pseudo-proper decay length (right) axes, for the J/ψ events in the kinematic bins given in the plots. The right panels show dimuons of invariant mass within $\pm 3\,\sigma_{CB}$ of the pole masses. The curves, identified in the legends, represent the result of the fits described in the text. The vertical bars on the data points show the statistical uncertainties.

and in the p_T ranges 10–95 GeV for the J/ψ and 10–75 GeV for the ψ(2S). A rapidity-integrated result in the range $|y|$<1.2 is also provided, extending the p_T reach to 120 GeV for the J/ψ and 100 GeV for the ψ(2S). The corresponding ψ(2S) over J/ψ cross section ratios are also reported. The dimuon invariant mass distribution is used to separate the J/ψ and ψ(2S) signals from other processes, mostly pairs of uncorrelated muons, while the dimuon decay length is used to separate the nonprompt charmonia, coming from decays of b hadrons, from the prompt component. Feed-down from decays of heavier charmonium states, approximately 33% of the prompt J/ψ cross section [21], is not distinguished from the directly produced charmonia.

The events were collected using a two-level trigger system. The first level, made of custom hardware processors, uses data from the muon system to select events with two muon candidates. The high-level trigger, adding information from the silicon tracker, reduces the rate of stored events by requiring an opposite-sign muon pair of invariant mass 2.8 < M < 3.35 GeV, p_T > 9.9 GeV, and $|y|$ < 1.25 for the J/ψ trigger, and 3.35 < M < 4.05 GeV and p_T > 6.9 GeV for the ψ(2S) trigger. No p_T requirement is imposed on the single muons at trigger level. Both triggers require a dimuon vertex fit χ^2 probability greater than 0.5% and a distance of closest approach between the two muons less than 5 mm. Events where the muons bend towards each other in the magnetic field are rejected to lower the trigger rate while retaining the highest-quality dimuons.

The analysis is restricted to muons produced within a fiducial phase-space window where the muon detection efficiencies are accurately measured: p_T > 4.5, 3.5, and 3.0 GeV for the regions $|\eta|$ < 1.2, 1.2 < $|\eta|$ < 1.4, and 1.4 < $|\eta|$ < 1.6, respectively. The combinatorial dimuon background is reduced by requiring a dimuon vertex fit χ^2 probability larger than 1%. After applying the event selection criteria, the combined yields of prompt and nonprompt charmonia in the range $|y|$ < 1.2 are 5.45 M for the J/ψ and 266 k for the ψ(2S). The prompt charmonia are separated from those resulting from decays of b hadrons through the use of the dimuon pseudo-proper decay length [22], $\ell = L_{xy}\,M/p_T$, where L_{xy} is the transverse decay length in the laboratory frame, measured after removing the two muon tracks from the calculation of the primary vertex position

For each ($|y|$, p_T) bin, the prompt charmonium yields are evaluated through an extended unbinned maximum-
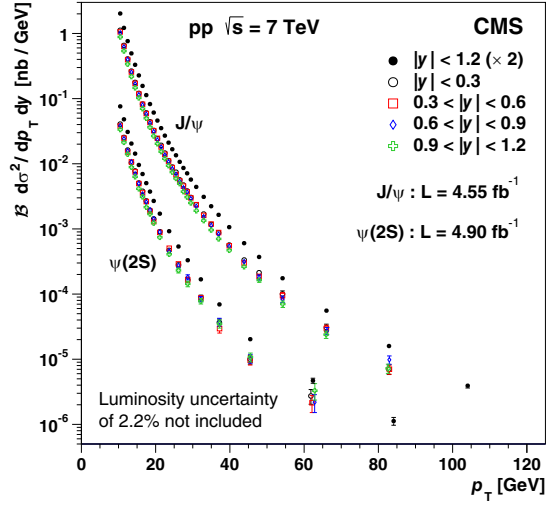
5

Figure 3: The J/ψ and ψ(2S) differential p_T cross sections times the dimuon branching fractions for four rapidity bins and integrated over the range $|y| < 1.2$ (scaled up by a factor of 2 for presentation purposes), assuming the unpolarized scenario. The vertical bars show the statistical and systematic uncertainties added in quadrature.

likelihood fit to the two-dimensional (M, ℓ) event distribution. In the mass dimension, the shape of each signal peak is represented by a Crystal Ball (CB) function [23], with free mean (μ_{CB}) and width (σ_{CB}) parameters. The mass distribution of the underlying continuum background is described by an exponential function. Concerning the pseudo-proper decay length variable, the prompt signal component is modeled by a resolution function, which exploits the per-event uncertainty information provided by the vertex reconstruction algorithm, while the nonprompt charmonium term is modeled by an exponential function convolved with the resolution function. The continuum background component is represented by a sum of prompt and nonprompt empirical forms. The distributions are well described with a relatively small number of free parameters. Figure 2 shows the J/ψ dimuon invariant mass and pseudo-proper decay length projections for a representative $(|\eta|, p_T)$ bin.

The double-differential cross sections of promptly produced J/ψ and ψ(2S) in the dimuon channel, $\mathcal{B}d^2\sigma/dp_Tdy$, where $\mathcal{B}$ is the J/ψ or ψ(2S) dimuon branching fraction, is obtained by dividing the fitted prompt-signal yields, already corrected on an event-by-event basis for efficiencies and acceptance, by the integrated luminosity and the widths of the p_T and $|y|$ bins. Figure 3 shows the results obtained in the unpolarized scenario. With respect to the $|y| < 0.3$ bin, the cross sections drop by $\approx 5\%$ for $0.6 < |y| < 0.9$ and $\approx 15\%$ for $0.9 < |y| < 1.2$. Measuring the charmonium production cross sections in the broader rapidity range $|y| < 1.2$ has the advantage that the increased statistical accuracy allows the measurement to be extended to higher-p_T values, where comparisons with theoretical calculations are particularly informative. Figure 4 compares the rapidity-integrated (unpolarized) cross sections, after rescaling with the branching fraction $\mathcal{B}$ of the dimuon decay channels [24], with results reported by ATLAS [18, 19]. The curve represents a fit of the J/ψ cross section measured in this analysis to a power-law function [25]. The band labelled FKLSW represents the result of a global fit [12] comparing SDCs calculated at NLO [9] with ψ(2S) cross sections and polarizations previously reported by CMS [16, 17] and LHCb [20]. According to that fit, ψ(2S) mesons are produced predominantly unpolarized. At high p_T, the values reported here tend to be higher than the
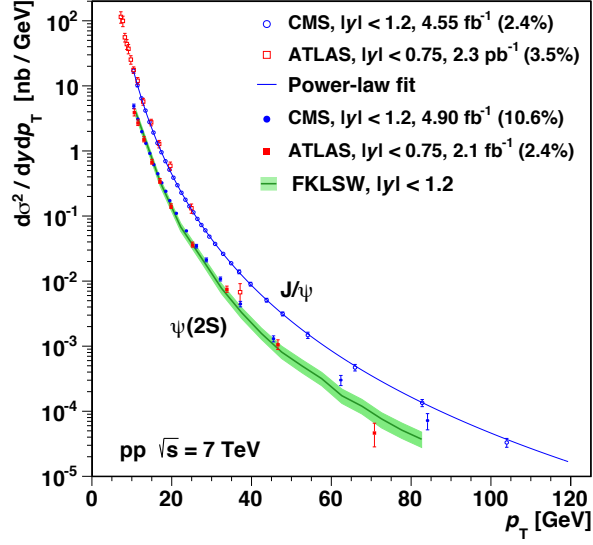
6

Figure 4: The J/ψ (open symbols) and $\psi(2S)$ (closed symbols) differential (unpolarized) cross sections from this analysis (circles) and from ATLAS (squares) [18, 19]. The vertical bars show the statistical and systematic uncertainties added in quadrature, not including the uncertainties from integrated luminosities and branching fractions, which are indicated by the percentages given in the legend. The curve shows a fit of the J/ψ cross section measured in this analysis to a power-law function, while the band labelled FKLSW represents a calculation of the $\psi(2S)$ cross section using LDMEs determined with lower-p_T LHC data [12].

band, which is essentially determined from results for $p_T < 30$ GeV.

In summary, the double-differential cross sections of the J/ψ and $\psi(2S)$ mesons promptly produced in pp collisions at $\sqrt{s} = 7$ TeV have been measured as a function of p_T in four $|y|$ bins, as well as integrated over the $|y| < 1.2$ range, extending up to or beyond $p_T = 100$ GeV. New global fits of cross sections and polarizations, including these high-p_T measurements, will probe the theoretical calculations in a kinematical region where NRQCD factorization is believed to be most reliable. The new data should also provide input to stringent tests of recent theory developments, such as those described in Refs. [26–28].

4   Measurement of the differential cross section for top quark pair production in pp collisions at $\sqrt{s}$ = 8 TeV

Understanding the production and properties of top quarks is fundamental for testing the quality of the standard model (SM) and for searching for new physical phenomena beyond its scope. Measurements of the top quark pair ($t\bar{t}$) production cross section as a function of ($t\bar{t}$) kinematic observables are important for comparing with QCD predictions within the SM, and thereby constrain QCD parameters. In addition, the top quark plays a relevant role in theories beyond the SM, and such differential measurements are therefore expected to be sensitive to new phenomena [29].

The first measurement of the normalized differential $t\bar{t}$ production cross section with the CMS detector at $\sqrt{s} = 8$ TeV is reported, uses data recorded in 2012 corresponding to an integrated luminosity of 19.7 $\pm$

7

0.5 fb^{-1}, which is about a factor of four larger than the sample used in the measurement performed by the CMS Collaboration at 7 TeV [30].

The measurements are performed in ℓ+jets channels ($\ell = e$ or μ), that contain a single isolated charged lepton and at least four jets in the final state, and in dilepton channels, with two oppositely charged leptons (ee, $\mu\mu$, $e\mu$) and at least two jets. The $t\bar{t}$ cross section is determined as a function of the kinematic properties of the top quarks and of the $t\bar{t}$ system, as well as of the leptons and jets associated with bottom (b) quarks (b jets) from top quark decays.

The results are compared to several predictions obtained with the leading-order (LO) *MADGRAPH* [31] generator interfaced to *PYTHIA* [32] for parton evolution and hadronization, the next-to-leading-order (NLO) generators *POWHEG* [33–35], interfaced to both *PYTHIA* and *HERWIG* [36], and *MCATNLO* [37] interfaced to *HERWIG*, and the latest NLO calculations with next-to-next-to-leading-logarithm (NNLL) corrections [38, 39], and approximate next-to-next-to-leading-order (NNLO) predictions [40].

Standard model background samples are simulated with *MADGRAPH* (without the *Madspin* package), *POWHEG*, or *PYTHIA6*, depending on the process. The main background contributions originate from the production of W and Z/γ^* bosons with additional jets (referred to as W+jets and Z+jets, respectively, in the following), single top quark (s-, t-, and tW channels), diboson (WW, WZ, and ZZ), $t\bar{t}$ production in association with a Z, W, or γ boson (referred to as $t\bar{t}$+Z/W/γ in the following), and QCD multijet events. The W+jets, Z+jets, and $t\bar{t}$+Z/W/γ samples are simulated with *MADGRAPH* with up to two additional partons in the final state. The *POWHEG* generator is used for simulating single top quark production, while *PYTHIA6* is used to simulate diboson and QCD multijet events. Parton showering and hadronization are also simulated with *PYTHIA6* in all the background samples. The *PYTHIA6* Z2* tune [42] is used to characterize the underlying event in both the $t\bar{t}$ and the background samples.

For comparison with the measured distributions, the event yields in the simulated samples are normalized to an integrated luminosity of 19.7 fb^{-1}, according to their predicted cross sections.

The top quark decays almost exclusively into a W boson and a b quark, and only the subsequent decays of one or two of the W bosons into a charged lepton (electron or muon) and a neutrino are considered. These signatures imply the presence of isolated leptons with high transverse momentum p_T, large p_T imbalance caused by the neutrinos that escape detection, and highly energetic jets. The identification of b jets through b-tagging techniques is used to increase the purity of the selected sample. The event selection in each channel is optimized to maximize the content of $t\bar{t}$ signal events and background rejection.

Events are reconstructed using a particle-flow technique, which combines signals from all subdetectors to enhance the reconstruction and identification of individual particles observed in pp collisions.

Electron candidates are reconstructed from a combination of the track momentum at the main interaction vertex, the corresponding energy deposition in the ECAL, and the energy sum of all bremsstrahlung photons attached to the track. The candidates are required to have $p_T > 33$ *GeV* within the pseudorapidity interval $|\eta| < 2.1$ for the ℓ+jets channels, while electron candidates in the dilepton channels are required to have $p_T > 20$ *GeV* and $|\eta| < 2.4$.

Jets are reconstructed by clustering the particle-flow candidates [43] using the anti-k_T clustering algorithm with a distance parameter of $R = 0.5$ [44]. Jets originating from b quarks are identified through a "combined secondary vertex" algorithm [45], which provides a b-tagging discriminant by combining secondary vertices and track-based lifetime information.

The missing transverse energy $\not{E}_T$ is defined as the magnitude of the imbalance in the transverse momentum $\vec{p}_T$ in the event, which is the negative of the vectorial sum of the momenta in the transverse plane of all the particles reconstructed with the particle-flow algorithm [46].

8

Events in the ℓ+jets channels that are triggered by the presence of a single electron (muon) with $p_T > 27\,GeV$ ($p_T > 24\,GeV$, $|\eta| < 2.1$), are selected if they contain exactly one reconstructed lepton fulfilling the requirements described above. In the dilepton channels, events are triggered using combinations of two leptons with p_T thresholds of 8 and 17 GeV, and are selected if they contain at least two isolated leptons of opposite electric charge and at least two jets. At least one of the jets is required to be b-tagged.

The kinematic properties of the top quark pair are determined from the four-momenta of all final-state objects through kinematic reconstruction algorithms.

Following the event selection and the kinematic reconstruction of the $t\bar{t}$ system, the main contributions to the background in the ℓ+jets channels arise from $t\bar{t}$ decays into channel other than ℓ+jets (including $t\bar{t}$ decays into τ leptons originating from the primary interaction) and single top quark events. The contribution from W+jets and QCD multijet events are well suppressed after the b-tagging requirement. A total of 24 927 events are found in the e+jets channel and 26 843 events in the μ+jets channel. The contribution from $t\bar{t}$ signal to the final event sample is 89.0%. The remaining fraction of events contains 7.3% $t\bar{t}$ decays other than the ℓ+jets channels, 2.4% single top quark events, 0.9% W+jets and $t\bar{t}$+Z/W/γ events, and negligible fractions of Z+jets, diboson, and QCD multijet events. All background contributions are determined from simulation.

In the dilepton channels, 10 678 events are found in the ee channel, 14 403 in the $\mu\mu$ channel, and 39 640 in the $e\mu$ channel. Only $t\bar{t}$ events containing at least two leptons (electrons or muons) from W decays in the final state are considered as signal, and constitute 79.0% of the final event sample. All other $t\bar{t}$ candidate events, specifically those originating from decays via τ leptons, are considered as background and amount to 13.3% of the final event sample. The fraction of Z+jets events is found to be 2.4%. This background, which is dominant to the ee and $\mu\mu$ channels, is estimated from data using the number of events observed within the Z-peak region (which is removed from the candidate sample), and a correction needed for non-Z+jets backgrounds in this same control region is obtained from data in the $e\mu$ channel [30]. Other sources of background, including single top quark production (3.4%), $t\bar{t}$+Z/W/γ production (1%), the contribution arising from misidentified or genuine leptons within jets (0.6%), or diboson events (0.3%), are estimated from simulation.

The measurement is affected by systematic uncertainties that originate from detector effects and from theoretical assumptions. The overall uncertainty on the measurement is obtained by adding all the contributions in quadrature, and is of the order of 3–10%, depending on the observable and the bin. The typical representative values of the systematic uncertainties in the normalized differential cross sections are summarized in Table 1.

The normalized $t\bar{t}$ cross section in each bin i of each observable X is determined as a function of the kinematic properties of the leptons, the lepton pair, the b jets, the b jet system, the lepton-b-jet system, the top quarks, and the $t\bar{t}$ system through the relation [30]:

$$\frac{1}{\sigma}\frac{\mathrm{d}\sigma_i}{\mathrm{d}X} = \frac{1}{\sigma}\frac{x_i}{\Delta_i^X \mathcal{L}} \tag{1}$$

where x_i represents the number of signal events measured in data after background subtraction and corrected for detector efficiencies, acceptances, and migrations, $\mathcal{L}$ is the integrated luminosity, and Δ_i^X is the bin width. The normalized differential cross section is obtained by dividing this quantity by the measured total cross section σ in the same phase space, which is evaluated by integrating over all bins for each observable X. The contribution to the background from other $t\bar{t}$ decays is taken into account, after subtracting all other background components, by correcting the number of signal events in data using the expected signal fraction. The expected signal fraction is defined as the ratio of the number of selected $t\bar{t}$ signal events

Table 1: Breakdown of typical systematic uncertainties for the normalized differential cross sections. The uncertainty on the jet-parton matching threshold is indicated as "ME-PS threshold". The medians of the distribution of uncertainties over all bins of the measurement are quoted. For the ℓ+jets channels, the background from Z+jets is negligible and included in the "Background (all other)" category.

	Relative systematic uncertainty (%)			
Source	Lepton and b jet observables		Top quark and $t\bar{t}$ observables	
	ℓ+jets	dileptons	ℓ+jets	dileptons
Trigger eff. & lepton selec.	0.1	0.1	0.1	0.1
Jet energy scale	2.3	0.4	1.6	0.8
Jet energy resolution	0.4	0.2	0.5	0.3
Background (Z+jets)	—	0.2	—	0.1
Background (all other)	0.9	0.4	0.7	0.4
b tagging	0.7	0.1	0.6	0.2
Kinematic reconstruction	—	<0.1	—	<0.1
Pileup	0.2	0.1	0.3	0.1
Fact./renorm. scale	1.1	0.7	1.8	1.2
ME-PS threshold	0.8	0.5	1.3	0.8
Hadronization	2.7	1.4	1.9	1.1
Top quark mass	1.5	0.6	1.0	0.7
PDF choice	0.1	0.2	0.1	0.5

to the total number of selected $t\bar{t}$ events (i.e. signal and all other $t\bar{t}$ events) in simulation. This procedure avoids the dependence on the total inclusive $t\bar{t}$ cross section used in the normalization of the simulated signal sample.

Effects from trigger and detector efficiencies and resolutions leading to the migration of events across bin boundaries, and therefore to statistical correlations among neighbouring bins, are corrected by using a regularized unfolding method [30, 47].

The measurement of the normalized differential cross sections proceeds as follows. For each kinematic distribution, the event yields in the separate channels are added together, the background is subtracted, and the unfolding is performed. It is verified that the measurements in separate channels yield results consistent within their uncertainties. The systematic uncertainties in each bin are determined from the changes in the combined cross sections.

Figure 5 presents the normalized differential cross section in the ℓ+jets channels as a function of the lepton transverse momentum p_T^l and the normalized differential cross sections for the dilepton channels as a function of the invariant mass $m_{l^+l^-}$ of the lepton pair.

The measurements in the different decay channels are in agreement with each other. In general, the data are in agreement with standard model predictions up to approximate NNLO precision. The *POWHEG+HERWIG6* prediction provides a good description of data for all measured distributions. However, the p_T spectrum in data for leptons, jets, and top quarks is softer than expected, particularly for *MADGRAPH+PYTHIA6*, *POWHEG+PYTHIA6*, and *MCATNLO+HERWIG6*. The calculation at approximate NNLO precision also provides a good description of the top quark p_T spectrum. The $m_{t\bar{t}}$ distribution in data tends to be lower than the predictions for large $m_{t\bar{t}}$ values. The $p_T^{t\bar{t}}$ spectrum is well described by all the considered predictions, except for the NLO+NNLL calculation, which fails to describe the data for all $p_T^{t\bar{t}}$ values. The results show the same behaviour as the corresponding CMS measurements at $\sqrt{s}$=7 TeV [30].
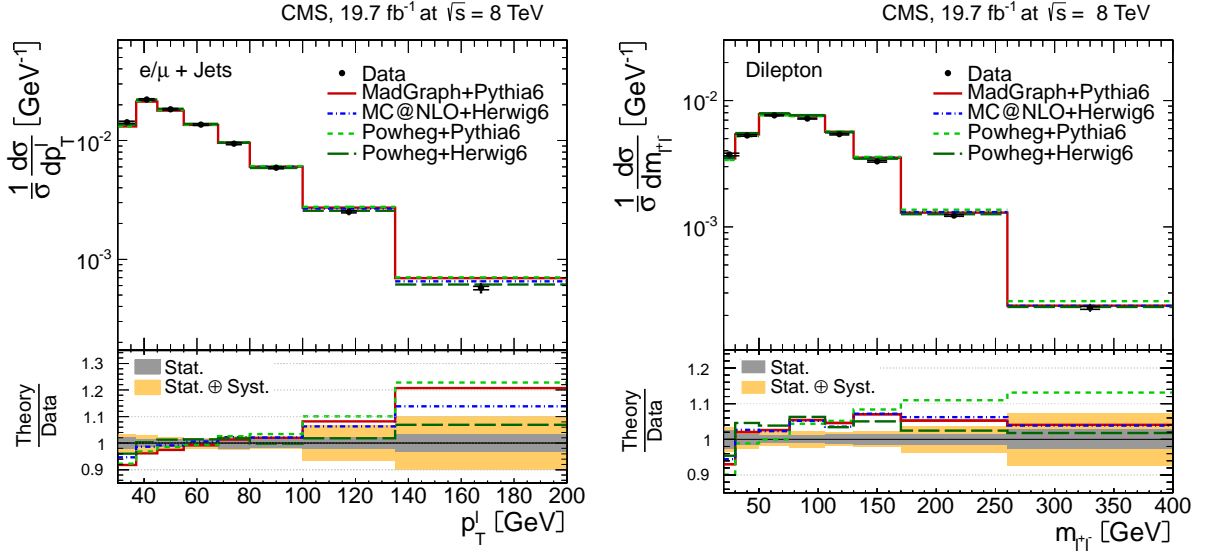
Figure 5: Normalized differential $t\bar{t}$ production cross section in the ℓ+jets channels as a function of the p_T^l of the charged lepton (left) and in the dilepton channels as a function of the $m_{l^+l^-}$ (right). The data points are placed at the midpoint of the bins. The inner (outer) error bars indicate the statistical (combined statistical and systematic) uncertainties. The measurements are compared to predictions from *MAD-GRAPH+PYTHIA6*, *POWHEG+PYTHIA6*, *POWHEG+HERWIG6*, and *MCATNLO+HERWIG6*. The lower part of each plot shows the ratio of the predictions to data.

5 Search for physics beyond the standard model in events with two leptons, jets, and missing transverse momentum in pp collisions at $\sqrt{s} = 8$ TeV

A search is presented for physics beyond the standard model (SM) in events containing a pair of opposite-sign same-flavor (SF) electrons or muons, jets, and an imbalance in transverse momentum. The search is based on a sample of proton-proton (pp) collisions collected at a center-of-mass energy of 8 TeV with the CMS detector at the CERN LHC in 2012 and corresponds to an integrated luminosity of 19.4 fb^{-1}.

The invariant mass distribution of the two-lepton system can exhibit an excess that increases with the dilepton mass, followed by a sharp decrease and thus an "edge", if the two leptons originate from the decay of an on-shell heavy neutral particle. This kind of signature is fairly generic for models of physics beyond the SM (BSM), assumes an isotropic decay, and is purely kinematic in origin. In models of SUSY [48], an edge with a triangular shape is expected in the cascade process $\widetilde{\chi}_2^0 \rightarrow \widetilde{\ell}\ell \rightarrow \widetilde{\chi}_1^0 \ell^+\ell^-$ [49], where $\widetilde{\chi}_2^0$ and $\widetilde{\chi}_1^0$ are respectively the next-to-lightest and lightest neutralino, with $\widetilde{\ell}$ a selectron or smuon, the SUSY partners of an electron or muon. Alternatively, the $\widetilde{\chi}_2^0$ can undergo a three-body decay to $\widetilde{\chi}_1^0 \ell^+\ell^-$ through a virtual Z^* boson, also yielding an edge in the dilepton mass spectrum but with a more rounded shape. Another possibility is the decay of a $\widetilde{\chi}_2^0$ to an on-shell Z boson, $\widetilde{\chi}_2^0 \rightarrow \widetilde{\chi}_1^0 Z$. This latter process does not produce an edge but rather a dilepton mass peak near 91 GeV. These processes arise as a consequence of the gauge-coupling structure of SUSY and are a characteristic feature of SUSY decay chains. Their relative importance depends
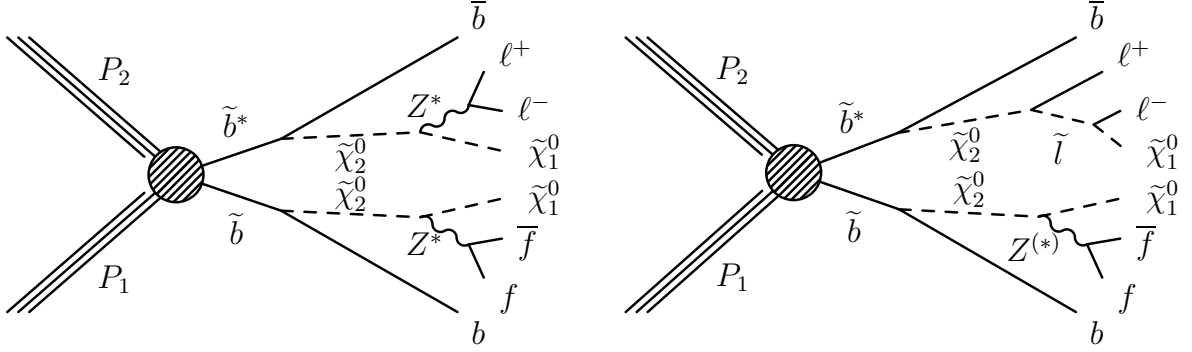
11

Figure 6: Event diagrams for the (left) "fixed-edge", and (right) "slepton-edge" scenarios, with $\widetilde{b}$ a bottom squark, $\widetilde{\chi}_2^0$ the second lightest neutralino, $\widetilde{\chi}_1^0$ a massive neutralino LSP, and $\widetilde{\ell}$ an electron- or muon-type slepton. For the slepton-edge scenario, the Z boson can be either on- or off-shell, while for the fixed-edge scenario it is off-shell.

on the SUSY mass hierarchy and is thus model dependent.

This search is therefore motivated by the possible existence of the fairly generic signal shape of an edge, or of a peak at the Z boson mass, that would be visible in the invariant mass distribution of the two leptons. The position of the edge would give an indication of the unknown BSM mass hierarchy.

The first class of signal events targets the production of an edge in the invariant mass spectrum of opposite-sign SF lepton pairs, as expected from the correlated production of these leptons in cascade decays. This class of scenarios is based on the production of a bottom squark-antisquark pair. Each bottom squark $\widetilde{b}$ decays to a bottom quark b and the $\widetilde{\chi}_2^0$ neutralino. Two specific possibilities are considered. In the first scenario (Fig. 6 left), the $\widetilde{\chi}_2^0$ decays to an off-shell Z boson Z^* and the $\widetilde{\chi}_1^0$ neutralino, where the $\widetilde{\chi}_1^0$ is a stable, weakly interacting, lightest SUSY particle (LSP). The Z^* boson decays according to its SM branching fractions, sometimes producing a charged lepton pair $\ell^+\ell^-$ ($\ell = e, \mu$). The mass difference between the $\widetilde{\chi}_2^0$ and $\widetilde{\chi}_1^0$, which determines the location of the edge, is fixed to 70 GeV. This scenario is referred to as the "fixed-edge" scenario. In the second scenario (Fig. 6 right), the $\widetilde{\chi}_2^0$ decays to an on- or off-shell Z boson and the $\widetilde{\chi}_1^0$ LSP or according to $\widetilde{\chi}_2^0 \to \ell\widetilde{\ell}$, with a 50% probability for each decay. The slepton $\widetilde{\ell}$, i.e., the SUSY partner of the lepton, then decays according to $\widetilde{\ell} \to \ell\widetilde{\chi}_1^0$. The considered sleptons are mass-degenerate selectrons and smuons. The mass of the slepton is chosen to lie halfway between the masses of the two neutralinos: $m_{\widetilde{\ell}} = m_{\widetilde{\chi}_1^0} + 0.5(m_{\widetilde{\chi}_2^0} - m_{\widetilde{\chi}_1^0})$. The mass of the $\widetilde{\chi}_1^0$ is set to 100 GeV, with the position of the edge a free parameter in a scan of the mass spectrum. This scenario is referred to as the "slepton-edge" scenario.

The second class of signal events targets the production of an opposite-sign SF lepton pair from the decay of an on-shell Z boson. This class of scenarios, illustrated in Fig. 7, is based on gluino pair production in the context of gauge mediated supersymmetry breaking (GMSB) models [50–52]. Each gluino decays to a quark-antiquark pair and the $\widetilde{\chi}_1^0$ neutralino. The $\widetilde{\chi}_1^0$ decays to an on-shell Z boson and a stable, massless, weakly interacting gravitino LSP. This scenario is referred to as the "GMSB" scenario.

The production of squark and gluino pairs is simulated with the *MADGRAPH5.1.3.30* [31] MC leading-order event generator, including up to two additional partons at the matrix element level. The decays of the squarks, gluinos, and other particles are simulated with the *PYTHIA6.4.22* [32] event generator. The *MADGRAPH* events are subsequently processed with the *PYTHIA* program to generate parton showers
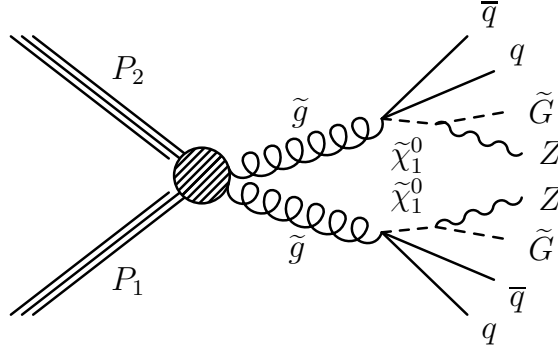
12

Figure 7: Event diagram for the "GMSB" scenario, with $\widetilde{g}$ a gluino, $\widetilde{\chi}_1^0$ the lightest neutralino, and $\widetilde{G}$ a massless gravitino LSP.

and account for hadronization. The decay of the Z boson is handled in *PYTHIA*. In all the aforementioned scenarios (fixed-edge, slepton-edge, GMSB), the Z boson decays according to its SM branching fractions. To reduce computational requirements, the detector response is simulated using the CMS fast simulation [53].

We select events with an oppositely charged lepton pair (e^+e^-, $e^\pm\mu^\mp$, or $\mu^+\mu^-$). The leptons are required to have $p_T > 20$ GeV and $|\eta| < 2.4$, where η is the pseudorapidity. In events with more than two selected leptons, we choose the two oppositely charged leptons with highest p_T.

The event selection criteria are motivated by the expectation that BSM signal events, involving the production of new heavy particles, generally have larger jet multiplicity and $\not{E}_T$ than background events, which primarily arise from top quark-antiquark ($t\bar{t}$) and Drell–Yan (DY) processes. The large value of $\not{E}_T$ expected in signal events is due to the weakly interacting LSP particles, which escape without detection.

In the search for an edge, two signal regions are defined: either $N_{\text{jets}} \geq 2$ and $\not{E}_T > 150$ GeV, or $N_{\text{jets}} \geq 3$ and $\not{E}_T > 100$ GeV. For both regions, there is a separate consideration for events in which both leptons satisfy $|\eta_{lep}| < 1.4$ ("central" signal region) and events in which at least one lepton satisfies $1.6 < |\eta_{lep}| < 2.4$ ("forward" signal region). The motivation for the distinction between the central and forward regions is that for BSM production through the decay of heavy resonances, the final-state leptons and jets are expected to be more centrally distributed than for the SM backgrounds. Two methods are used to search for an edge signature. In the first method, a search for an edge is performed in the range $20 < m_{ll} < 300$ GeV by fitting the signal and background hypotheses to data. In the second method, based on a direct comparison of event counts, with no assumption about the shapes of the signal and background distributions, three regions are selected , $20 < m_{ll} < 70$ GeV, $81 < m_{ll} < 101$ GeV, and $m_{ll} > 120$ GeV, denoted the "low-mass", "on-Z", and "high-mass" regions, respectively. For this "counting experiment", the integrated yield in each region is compared to the corresponding background prediction.

In the search for BSM events with an on-shell Z boson, a dedicated counting experiment is performed in the region $81 < m_{ll} < 101$ GeV. For this study, two inclusive bins in the number of jets are defined: $N_{\text{jets}} \geq 2$ and $N_{\text{jets}} \geq 3$. Events are examined in exclusive bins of $\not{E}_T$.

The principal SM backgrounds are divided into two categories. Backgrounds that produce OF pairs ($e^+\mu^-$, $e^-\mu^+$) as often as SF pairs (e^+e^-, $\mu^+\mu^-$) are referred to as flavor-symmetric (FS) backgrounds. This category is dominated by $t\bar{t}$ processes. Drell–Yan events form the second principal background category. The FS background estimate accounts also for WW, $Z/\gamma^*(\to \tau\tau)$, and tW single-top quark production, as well as for

13

backgrounds due to leptons from hadron decays and from hadrons misidentified as leptons. Contributions from $t\bar{t} + X$, with X a W, Z, or Higgs boson, have been studied in the simulation and found to be negligible.

The missing transverse momentum in DY+jets events arises primarily from jet energy resolution and reconstruction effects. Contributions from SM WZ and ZZ processes, which might include genuine $\not{E}_T$, are incorporated into the DY+jets background estimates.

Figure 8 shows the invariant mass distributions for the signal candidate sample and the estimated background.
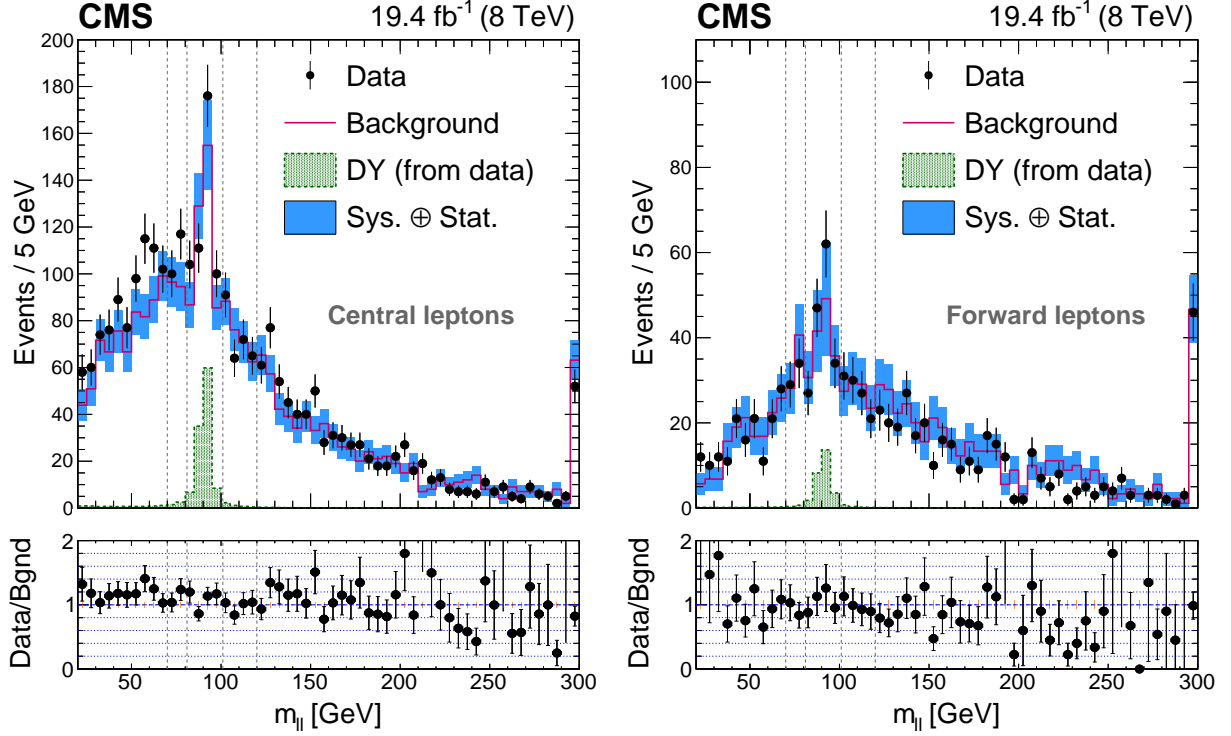

Figure 8: Comparison between the observed and estimated SM background dilepton mass distributions in the (left) central and (right) forward regions, where the SM backgrounds are evaluated from control samples. The rightmost bins contain the overflow. The vertical dashed lines denote the boundaries of the low-mass, on-Z, and high-mass regions. The lower plots show the ratio of the data to the predicted background. The error bars for both the main and lower plots include both statistical and systematic uncertainties.

The significance of the excess in the observed number of events with respect to the estimated number of SM background events is evaluated using a profile likelihood asymptotic approximation. The local significance of the excess in the central low-mass region, where the largest deviation is found, is 2.6 standard deviations. Note that the signal regions were defined before the data sample was examined, and that the low-mass region ($20 < m_{ll} < 70$ GeV) does not include events between 70 GeV and the best-fit value for the location of the edge (m_{ll}=78.7 GeV). The flavor of the $\ell^+\ell^-$ pair was studied in the counting experiment. Within the statistical uncertainty and accounting for differences in the reconstruction efficiencies, the electron and the muon channels are found to contribute evenly to the excess. Further studies of the excess in the low-mass region do not yield evidence for a neglected systematic term. The excess is observed predominantly in

events with at least one identified bottom quark jet (b jet) and diminishes if a veto on the presence of a b jet is applied. To identify b jets, the CSV algorithm at the medium working point [54] is used.

Searches are performed for signals that either produce a kinematic edge, or a peak at the Z boson mass, in the dilepton invariant mass distribution. For regions dominated by flavor-symmetric backgrounds, i.e., backgrounds that produce opposite-flavor events $e^+\mu^-, e^-\mu^+$ as often as same-flavor events $e^+e^-, \mu^+\mu^-$, a precision of about 5% (10%) is reached for the estimated number of standard model background events in the central (forward) lepton rapidity regions. No evidence is observed for a statistically significant signal. The maximum deviation from the null hypothesis is at the level of 2.6 standard deviations and is observed in the dilepton mass window $20 < m_{ll} < 70$ GeV.

The results of the search for a kinematic edge is interpreted in the context of simplified models consisting of bottom-squark pair production, with each bottom-squark $\widetilde{b}$ decaying to a bottom quark and the $\widetilde{\chi}_2^0$ neutralino. Exclusion limits are set in the $m_{\widetilde{b}}$-$m_{\widetilde{\chi}_2^0}$ mass plane for two scenarios. In the fixed-edge scenario, the mass difference between the $\widetilde{\chi}_2^0$ and $\widetilde{\chi}_1^0$ particles is fixed to 70 GeV. Bottom-squark masses between 200 and 350 GeV are excluded at 95% confidence level in this scenario. In the slepton-edge scenario, the $\widetilde{\chi}_2^0$ decays to an on- or off-shell Z boson and the $\widetilde{\chi}_1^0$ lightest supersymmetric particle or to a slepton and a lepton, with a 50% probability for each possibility. Bottom-squark masses between 450 and 600 GeV are excluded at 95% confidence level in this second scenario. In both scenarios, the sensitivity depends on the mass of the $\widetilde{\chi}_2^0$. Finally, a dedicated search for events containing an on-shell Z boson is interpreted in a model of gauge-mediated supersymmetry breaking, in which the Z bosons are produced in decay chains initiated through gluino pair production. Gluino masses between 900 and 1100 GeV are excluded at 95% confidence level, depending on the mass of the lightest neutralino $\widetilde{\chi}_1^0$.

References

[1] CMS Collaboration, *JINST* **3** S08004 (2008).

[2] Bobeth, C. *et al.*, *Phys. Rev. Lett.* **112**, 101801 (2014).

[3] Evans, L. and Bryant, P., *J. Instrum.* **3**, S08001 (2008).

[4] Breiman, L., Friedman, J. H., Olshen, R. A., and Stone, C. J., *Classification and Regression Trees*.

[5] Freund, Y. and Schapire, R. E. A., *J. Comput. Syst. Sci.* **55**, 119–139 (1997).

[6] Hoecker, A. *et al.*, *PoS* **ACAT**, 040 (2007) .

[7] N. Brambilla *et al.*, *Eur. Phys. J. C* **71** 1534 (2011).

[8] G. T. Bodwin, E. Braaten, and G. P. Lepage, *Phys. Rev. D* **51** 1125 (1995).

[9] M. Butenschoen and B. A. Kniehl, *Phys. Rev. Lett.* **108** 172002 (2012).

[10] B. Gong, L.-P. Wan, J.-X. Wang, and H.-F. Zhang, *Phys. Rev. Lett.* **110** 042002 (2013).

[11] K.-T. Chao *et al.*, *Phys. Rev. Lett.* **108** 242004 (2012) .

[12] P. Faccioli *et al.*, *Phys. Lett. B* **736** 98 (2014).

[13] CDF Collaboration, *Phys. Rev. Lett.* **99** 132001 (2007).

[14] CDF Collaboration, *Phys. Rev. Lett.* **108** 151802 (2012).

[15] CMS Collaboration, *Phys. Rev. Lett.* **110** 081802 (2013).

[16] CMS Collaboration, *Phys. Lett. B* **727** 381 (2013).

[17] CMS Collaboration, *JHEP* **02** 011 (2012).

[18] ATLAS Collaboration, *Nucl. Phys. B* **850** 387 (2011).

[19] ATLAS Collaboration, *JHEP* **09** 079 (2014).

[20] LHCb Collaboration, *Eur. Phys. J. C* **72** 2100 (2012).

[21] P. Faccioli, C. Lourenço, J. Seixas, and H. Wöhri, *JHEP* **10** 004 (2008).

[22] CMS Collaboration, *Eur. Phys. J. C* **71** 1575 (2011).

[23] M. J. Oreglia, PhD thesis, Stanford University, 1980. SLAC-R-236.

[24] Particle Data Group, K. A. Olive et al., *Chin. Phys. C* **38** 090001 (2014).

[25] HERA-B Collaboration, *Eur. Phys. J. C* **49** 545 (2007).

[26] Z.-B. Kang, J.-W. Qiu, and G. Sterman, *Phys. Rev. Lett.* **108** 102002 (2012).

[27] Z.-B. Kang, Y.-Q. Ma, J.-W. Qiu, and G. Sterman, *Phys. Rev. D* **90** 034006 (2014).

[28] G. T. Bodwin, H. S. Chung, U.-R. Kim, and J. Lee, *Phys. Rev. Lett.* **113** 022001 (2014).

[29] R. Frederix and F. Maltoni, *JHEP* **01** 047 (2009).

[30] CMS Collaboration, *Eur. Phys. J. C* **73** 2339 (2013).

[31] J. Alwall et al. *JHEP* **06** 128 (2011).

[32] T. Sjöstrand, S. Mrenna, and P. Skands, *JHEP* **05** 026 (2006).

[33] S. Alioli et al. *JHEP* **09** 111 (2009).

[34] S. Alioli et al., *JHEP* **06** 043 (2010).

[35] E. Re, *Eur. Phys. J. C* **71** 1547 (2011).

[36] G. Corcella et al. *JHEP* **01** 010 (2001).

[37] S. Frixione and B. R. Webber, *JHEP* **06** 29 (2002).

[38] A. Ferroglia, B. D. Pecjak, and L. L. Yang, *JHEP* **09** 032 (2013).

[39] H. T. Li et al., *Phys. Rev. D* **88** 074004 (2013).

[40] N. Kidonakis, *Phys. Part. Nuclei* **45** 714 (2014).

[41] H.-L. Lai et al., *Phys. Rev. D* **82** 074024 (2010).

[42] CMS Collaboration, *JHEP* **09** 109 (2011).

[43] CMS Collaboration, *JINST* **6** P11002 (2011).

[44] M. Cacciari, G. P. Salam, and G. Soyez, *JHEP* **04** 063 (2008).

[45] CMS Collaboration, *JINST* **8** P04013 (2013).

[46] CMS Collaboration, *JINST* **6** P09001 (2011).

[47] A. Hoecker and V. Kartvelishvili, *Nucl. Instrum. Meth. A* **372** 469 (1996).

[48] S. P. Martin, *Adv. Ser. Direct High Energy Phys.* **21** 1 (2010).

[49] I. Hinchliffe et al., *Phys. Rev. D* **55** 5520 (1997).

[50] K. T. Matchev and S. D. Thomas, *Phys. Rev. D* **62** 077702 (2000).

[51] P. Meade, M. Reece, and D. Shih, *JHEP* **05** 105 (2010).

[52] J. T. Ruderman and D. Shih, *JHEP* bf08 159 (2012).

[53] S. Abdullin et al., *Intl. Conf. on Computing in High Energy and Nuclear Physics* (CHEP 2010).

[54] CMS Collaboration, *JINST* **8** P04013 (2013).